Journal of Physics D: Applied Physics

PURPOSE-LED PUBLISHING™

PAPER · OPEN ACCESS

Secondary electron emission measurements from imidazolium-based ionic liquids

To cite this article: A M Capece and A N Enriquez 2025 *J. Phys. D: Appl. Phys.* **58** 035206

OPEN ACCESS
IOP Publishing
Journal of Physics D: Applied Physics
J. Phys. D: Appl. Phys. **58** (2025) 035206 (6pp)
https://doi.org/10.1088/1361-6463/ad89d7

Secondary electron emission measurements from imidazolium-based ionic liquids

A M Capece* and **A N Enriquez**

The College of New Jersey, 2000 Pennington Road, Ewing, NJ 08628, United States of America

E-mail: capecea@tcnj.edu

Received 14 August 2023, revised 13 October 2024
Accepted for publication 22 October 2024
Published 1 November 2024

Abstract

The electron-induced secondary electron emission (SEE) yields of imidazolium-based ionic liquids are presented for primary electron beam energies between 30 and 1000 eV. These results are important for understanding plasma synthesis of nanoparticles in plasma discharges with an ionic liquid electrode. Due to their low vapor pressure and high conductivity, ionic liquids can produce metal nanoparticles in low-pressure plasmas through reduction of dissolved metal salts. In this work, the low vapor pressure of ionic liquids is exploited to directly measure SEE yields by bombarding the liquid with electrons and measuring the resulting currents. The ionic liquids studied are [BMIM][Ac], [EMIM][Ac], and [BMIM][BF_4]. The SEE yields vary significantly over the energy range, with maximum yields of around 2 at 200 eV for [BMIM][Ac] and [EMIM][Ac], and 1.8 at 250 eV for [BMIM][BF_4]. Molecular orbital calculations indicate that the acetate anion is the likely electron donor for [BMIM][Ac] and [EMIM][Ac], while in [BMIM][BF_4], the electrons likely originate from the [BMIM]$^+$ cation. The differences in SEE yields are attributed to varying ionization potentials and molecular structures of the ionic liquids. These findings are essential for accurate modeling of plasma discharges and understanding SEE mechanisms in ionic liquids.

Keywords: secondary electron emission, ionic liquids, nanoparticle synthesis

1. Introduction

Ionic liquids are salts that consist of an organic cation and either a simple or polyatomic anion, and they are typically liquid at or near room temperature. These liquids are chemically stable and nonvolatile, making them useful for a variety of applications including electrochemical devices, nanoparticle synthesis, catalysis, and green chemistry [1, 2]. As a result of their low vapor pressure, ionic liquids can be used with low pressure plasmas to produce metal nanoparticles through the reduction of dissolved metal salts by the reactive species (including ions, electrons, and radicals) produced in the plasma [3–5]. For example, liquids seeded with gold compounds have been shown to form gold nanotubes and other nanostructures when in contact with a plasma [6, 7]. The ionic liquid stabilizes the metal nanoparticles and prevents agglomeration through electrosteric stabilization of the metal nanoparticles, which occurs as a result of the liquid's Coulomb network of charges [8]. Ionic liquids present an advantage over other media for nanoparticle synthesis because additional reducers and stabilizers are not needed, and the low volatility of ionic liquids makes them suitable for use with low pressure plasmas [3]. Ionic liquids containing imidazolium-based cations, such as 1-butyl-3-methylimidazolium (BMIM)

* Author to whom any correspondence should be addressed.

and 1-ethyl-3-methylimidazolium (EMIM), are preferred for metal electrodeposition because of their high conductivity [9]. Previous studies have shown imidazolium-based ionic liquids to be important for shape-controlled synthesis of silver crystals with hierarchical structures [10].

Metal nanoparticles can be synthesized in ionic liquids during exposure to a plasma discharge generated between a metal electrode and an ionic liquid solution containing dissolved metal precursors [8, 11]. Chen *et al* measured the voltage and current of a DC discharge operating with an ionic liquid electrode and found that at low pressures (< 3 Torr), the discharge parameters were dominated by secondary electron emission (SEE) from the electrode [12]. SEE occurs when a material liberates electrons as a result of bombardment by incident electrons and ions, and the SEE yield is defined as the ratio of the number of emitted electrons to the number of incident particles. SEE is important for breakdown in plasma discharges, and it sustains the plasma and stabilizes the discharge current. Since the SEE yield is material dependent, the discharge current in the plasma is heavily influenced by which ionic liquid is used.

Horváth *et al* performed particle-in-cell/Monte Carlo collisions simulations to understand the influence of electron-induced secondary electrons on capacitively-coupled oxygen and argon plasmas at low pressures [13, 14]. They found that using energy-dependent yield values, rather than considering a fixed yield, significantly changed their simulations results. The plasma exhibited a marked increase in the electron density and improved ionization dynamics when they included realistic, energy-dependent values of electron-induced SEE yields into their models. They also showed that in radio frequency discharges, the ion-induced secondary electrons from one electrode can be accelerated by the sheath into the bulk plasma and reach the opposite electrode, where they can induce secondary electrons. This conclusion is consistent with the findings of Baba *et al* [15], who investigated RF discharges operating with an ionic liquid electrode. Their setup included a stainless steel mesh electrode inside a Teflon cell. They observed that the electron density in the plasma increased by more than a factor of two when the ionic liquid was introduced. They attributed this increase to enhanced SEE from the ionic liquid. These studies highlight the importance of using energy-dependent values of the SEE yields to obtain accurate simulation results. Indeed as seen by Chen *et al* [12] and Kaneko [16, 17], the high SEE yield of ionic liquids seems to enhance ionization in the plasma, leading to higher discharge currents and lower breakdown voltages compared with metal electrodes.

SEE measurements from liquids are difficult because electron gun operation requires low pressures, typically less than 10^{-6} Torr, which is often below the vapor pressure of most liquids. In many cases, the SEE yield from materials used in plasma applications is inferred from breakdown measurements and I-V curves. For example, Delgado *et al* [18]. estimated the SEE yield of water using an electrochemical reactor in which an argon plasma functioned as one electrode and a platinum foil submerged in the liquid was used as the opposite electrode. They obtained a SEE yield of $< 10^{-5}$ for water by using the Paschen model to determine the yield that provided the best fit to their measurements of the breakdown voltage. Oyarzabal and Tabares [19] measured electron-induced SEE yields of liquid lithium for electron energies up to 150 V using I-V curves obtained during operation of a 5-mTorr helium DC glow discharge, and Kvon *et al* [20]. performed similar SEE studies on molten Sn-Li.

Kaneko *et al* [16] measured the I-V curve for an argon DC plasma ignited between a grounded stainless steel anode and a platinum cathode submerged in 3 ml of [BMIM][BF_4]. The discharge current was highest using an ionic liquid electrode compared with experiments using nickel and stainless steel electrodes. These results indicate that the SEE yield of [BMIM][BF_4] is higher than both nickel and stainless steel, and Chen *et al* [12] estimated the SEE yield of [BMIM][BF_4] to be 1 from Kaneko's measurements. Using the Paschen model or I-V curves to estimate SEE gives only one yield value and lacks information on how the yield changes with incident particle energy. In the experiments presented here, direct measurements of the total electron yield (TEY) of [BMIM][BF_4] were obtained by bombarding the liquid under vacuum with primary electrons of energies between 30 and 1000 eV and measuring the resulting SEE current. By performing direct measurements rather than inferring the yields from breakdown models, accurate measurements over a large energy range applicable for glow discharges can be obtained. In this work, direct measurements of the SEE yield for three imidazolium-based ionic liquids are presented for primary electron energies of 30-1000 eV. The liquids include: 1-butyl-3-methylimidazolium acetate ([BMIM][Ac]), 1-ethyl-3-methylimidazolium acetate ([EMIM][Ac]), and 1-butyl-3-methylimidazolium tetrafluoroborate ([BMIM][BF_4]). The structural formulas of each of these ionic liquids are shown in figure 1.

2. Experimental setup

SEE measurements were conducted in a stainless steel vacuum chamber with a base pressure of 7×10^{-8} Torr at the Princeton Collaborative Low Temperature Plasma Research Facility (PCRF) at Princeton Plasma Physics Laboratory. The vacuum chamber is equipped with a fast entry load-lock door for easy access to the sample and a Kimball Physics ELG-2 electron gun that produces primary electron energies up to 1000 eV. The sample stage is mounted on a linear feedthrough and contains a stainless steel cup 0.8 inch in diameter and 0.1 inch deep to hold the liquid sample. The ionic liquid used were [BMIM][Ac] ($\geqslant 96.0\%$, Sigma-Aldrich), [EMIM][Ac] (97.0%, Sigma-Aldrich), and [BMIM][BF_4] (97.0%, Sigma-Aldrich), which have conductivities of 1.44 mS cm^{-1} (at 25°C) [21], 2.776 mS cm^{-1} (at 25°C) [22], and 3.3 mS cm^{-1} (at 30°C) [23], respectively. Fluorinated ionic liquids with imidazolium-based cations such as [BMIM]$^+$ have the high electrical conductivity necessary

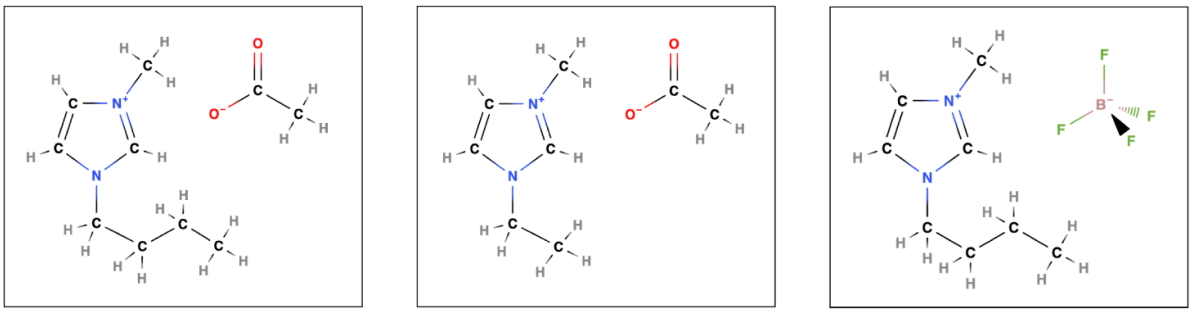

(a) [BMIM][Ac] (b) [EMIM][Ac] (c) [BMIM][BF_4]

Figure 1. Structural formulas for the three ionic liquids considered in this study.

for the dissipation of electrical charge when exposed to high energy electron beam irradiation. In addition, the vapor pressure of ionic liquids is negligible, making vacuum-based measurements viable. The stainless steel cup was cleaned with acetone and alcohol before use and approximately 0.5 ml of the liquid was placed in the cup using a pipette. The stage also contains a Faraday cup in order to easily characterize the electron beam and ensure that it is aligned with the sample during experiments. The beam diameter during these measurements was approximately 0.5 mm.

Current measurements were collected using a Keithley 6485 picoammeter. The beam current, I_{beam}, was measured by biasing the sample to +70 V to collect all primary electrons and suppress secondary electrons. Beam currents ranged between 60 and 800 nA for all experiments. The total electron emission current, which includes both secondary and backscattered electrons, was obtained by measuring the current to the sample, I_{sample}, without the +70-V bias and subtracting it from the beam current. For these measurements, the sample was grounded through the picoammeter and a +20-V bias was placed on a cylindrical collector located above and axisymmetric with the sample. The collector was isolated from the electron gun and was used to attract the secondary electrons away from the sample. A +20 V bias was chosen for the cylindrical collector based on the energy of secondary electrons (typically below 50 eV) to ensure effective collection without distorting the sample measurements. The sample current measurement consists of both the primary electron beam current and the secondary electron current such that

$$I_{\text{see}} = I_{\text{beam}} - I_{\text{sample}}. \tag{1}$$

The total secondary electron yield is therefore:

$$\gamma = \frac{I_{\text{see}}}{I_{\text{beam}}} = \frac{I_{\text{beam}} - I_{\text{sample}}}{I_{\text{beam}}} = 1 - \frac{I_{\text{sample}}}{I_{\text{beam}}}. \tag{2}$$

Schematics of the two different configurations used to measure beam and sample currents are shown in figures 2(a) and (b), respectively.

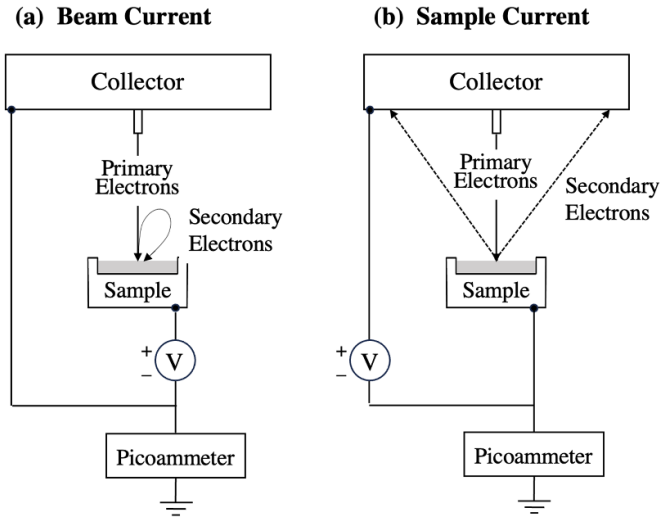

Figure 2. Schematic of the secondary electron emission experiment at PCRF. The left diagram shows the configuration for measuring the beam current. The right diagram shows the configuration for measuring the sample current, which is equivalent to the beam current less the secondary electron emission current.

3. Results and discussion

The total electron yields of the three liquids are shown in figures 3 and 4 as a function of primary electron energy from 30 to 1000 eV. The average yields for each of the three liquids are shown together in figure 3 without error bars for clarity and ease of comparison. Error bars are shown in figure 4 and represent one standard deviation of uncertainty for $N = 4$ experiments. The error accounts for instrumentation error of the Keithley 6485 picoammeter and the systematic error caused by currents that do not fully saturate. The total electron yield exceeds one for incident electron energies above 50 eV and reaches its maximum value at an electron energy of 200 eV for [BMIM][Ac] and [EMIM][Ac] and 250 eV for [BMIM][BF_4].

The yield measurements are compared with a model proposed by Scholtz *et al* [24] in which the yield is described by

$$\gamma = \gamma_m \exp\left[-\frac{\left(\ln\frac{E}{E_m}\right)^2}{2\sigma^2}\right], \tag{3}$$

where E is the primary electron energy, σ is a fit parameter, and γ_m and E_m refer to the maximum yield and the corresponding

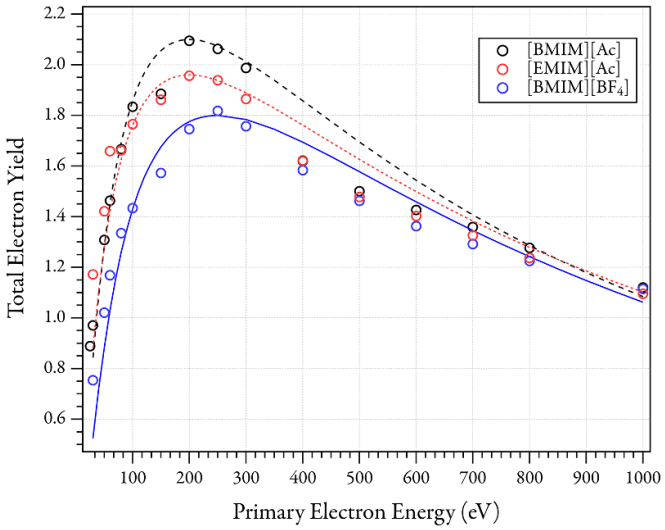

Figure 3. Measurements of the total electron yield as a function of primary electron energy. The lines are fits of the universal yield curve proposed by Scholtz *et al* [24].

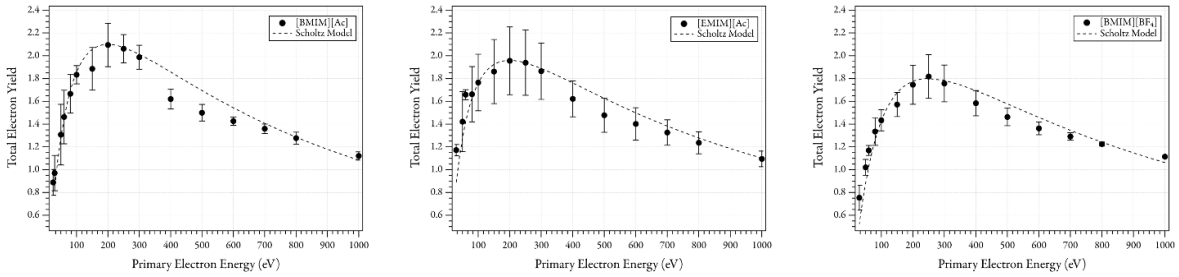

(a) TEY for [BMIM][Ac]. (b) TEY for [EMIM][Ac] (c) TEY [BMIM][BF_4]

Figure 4. Measurements of the total electron yield for each liquid as a function of primary electron energy.

energy value, respectively. The lines in figures 3 and 4 represent fits of equation (3) to the yield data. The corresponding fit parameters are listed in table 1. As seen in figure 3, the SEE yield varies considerably with energy from 30 to 1000 eV, which is in the range of most discharges. The yield exceeds 1 for most of the energy range, and it exceeds 1.5 between 100 and 600 V. The Scholtz model predicts that the yield will drop below one for electron energies above 1000 eV.

For energies up to approximately 100 eV, [BMIM][Ac] and [EMIM][Ac] display coinciding TEY values, but they start to diverge beyond this point. The most significant differences in TEY values for all three liquids occur in the energy range of about 100 to 400 eV. The TEY of all three ionic liquids converges for energies of 400 eV and above. Among the three, [BMIM][Ac] exhibits the highest yield, reaching a maximum of 2.1. [EMIM][Ac] follows with a maximum yield of 1.96, and [BMIM][BF_4] has the lowest maximum yield at 1.8.

There is some evidence that the length of the alkyl chain may account for the difference in TEY between [BMIM][Ac] and [EMIM][Ac]. Rivera-Rubero and Baldelli performed surface characterization of different ionic liquids with the $[BMIM]^+$ cation using sum frequency generation spectroscopy and determined that the imidazolium ring lays flat along the surface and the butyl chain extends into the gas phase [25]. This orientation suggests a potential drop between the vacuum and the bulk liquid. Kaneko *et al* operated a plasma discharge using ionic liquids with alkyl chains of different lengths and interchanged butyl, a four-carbon alkyl group, in [BMIM][BF_4] for ethyl and hexyl, which are two- and six-carbon alkyl groups, respectively [17]. They found that the discharge current increased when ionic liquids with larger alkyl chains were used. They concluded that the orientation of the alkyl chain may increase the electric field in the cathode sheath to generate larger SEE currents.

Our experimental results align with these findings. We observed that the yield of [BMIM][Ac] exceeds that of [EMIM][Ac], indicating that the longer alkyl chain in $[BMIM]^+$ (butyl group with 4 carbons) results in higher yields compared to the shorter alkyl chain in $[EMIM]^+$ (ethyl

Table 1. table of fit parameters to the Universe yield curve proposed by Scholtz *et al* [24] for each ionic liquid.

Ionic Liquid	γ_{max}	E_{max}	σ
[BMIM][Ac]	2.1	200 eV	1.4
[EMIM][Ac]	1.96	200 eV	1.5
[BMIM][BF_4]	1.8	250 eV	1.35

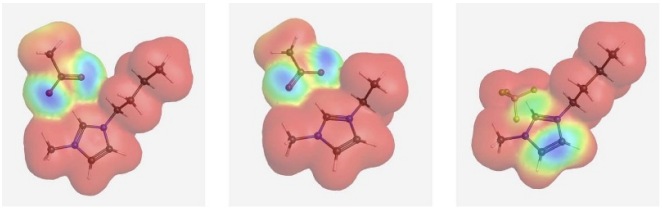

(a) [BMIM][Ac] (b) [EMIM][Ac] (c) [BMIM][BF_4]

Figure 5. The optimized structure and electrophilic frontier density plot of each ionic liquid using Hartree–Fock theory with a 6-31G(d) basis set.

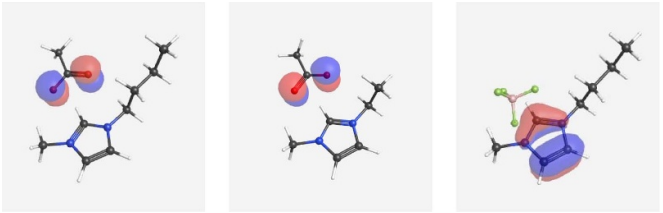

(a) [BMIM][Ac] (b) [EMIM][Ac] (c) [BMIM][BF_4]

Figure 6. Molecular orbital plot of each ionic liquid for the HOMO surface.

group with 2 carbons), while both have the same anion. However, [BMIM][BF_4] shows the lowest yields, suggesting that the anion also plays a significant role in determining the yield.

To help distinguish differences in SEE between the three liquids, we generated electrophilic frontier density plots, shown in figure 5, which give the most probable location of an electrophilic attack on, or the loss of, an electron from a molecule. We also generated molecular orbital plots for the highest occupied molecular orbital (HOMO) for each liquid, shown in figure 6. The geometry of the ionic liquid was optimized using Gaussian16 [26] and Hartree–Fock theory with a 6-31G(d) basis set. Following optimization, a molecular orbitals calculation was performed and the Fukui f^- function was used to calculate the electrophilic frontier density. The electrophilic frontier density plots and the HOMO for each liquid were visualized using WebMO [27] to create isosurface representations. These visualizations highlight regions of the molecule with high electron density, indicating likely sources of emitted electrons and revealing where electrons might originate during SEE. In frontier density plots, blue represents the highest probability of electrophilic attack (i.e. the donation of an electron from the molecule), while red represents the lowest probability. From figure (5) of [BMIM][Ac] and [EMIM][Ac], it is evident that the electrons are most likely to come from the $[Ac]^-$ anion. Conversely, in [BMIM][BF_4], the electrons are more likely to originate from the imidazolium ring of the $[BMIM]^+$ cation.

The HOMO energies were calculated and are listed in table 2 along with values from previous computational studies. According to Koopmans' theorem, the ionization potential (IP) of a molecule is approximately equal to the negative of the energy of the HOMO in the Hartree–Fock approximation [31]. Since the SEE yield of a material is dependent on its IP, variations in HOMO energy and IP could help explain relative differences between the yields of different materials. We calculate the HOMO energy of $[BMIM]^+$ to be greater than $[EMIM]^+$, which is consistent with results from Ilawe *et al* [29]. This suggests that it is easier to remove an electron from $[BMIM]^+$ over $[EMIM]^+$. In addition, our results show that the HOMO energies for [BMIM][Ac] and [EMIM][Ac] are very similar at around 9.1 eV, which could also support the previously stated conjecture that the orientation of the ionic liquid at the liquid-vacuum interface plays an important role in SEE by creating a potential drop that depends on alkyl chain length.

Table 2. Ionization potential and HOMO energies.

Ion/Ionic Liquid	IP (eV)	HOMO (eV)
$[BMIM]^+$	4.072[a], 12.40[b]	−11.698[a], −14.18[c]
$[EMIM]^+$	6.976[a], 12.53[b]	−11.820[a], −14.29[c]
BF_4^-	8.44[b]	−9.55[c]
$CH_3CO_2^-$	1.79[b]	−4.35[c]
[BMIM][Ac]	—	−9.09[c], −7.36[d]
[EMIM][Ac]	—	−9.06[c]
[BMIM][BF_4]	—	−10.7[c], −9.42[d]

[a] Gupta *et al* [28].
[b] Ilawe *et al* [29].
[c] This work.
[d] Bardak *et al* [30].

Our measurements show that [BMIM][BF_4] has the lowest TEY, suggesting that the anion significantly influences the yield. This observation is consistent with the frontier density plots, which indicate that the acetate anion, with its lower IP, is identified as the probable electron donor for [BMIM][Ac]. Conversely, in [BMIM][BF_4], the $[BMIM]^+$ cation, which has a higher IP, is the likely source of electrons. This distinction implies that electron donation is more favorable from the acetate in comparison to $[BMIM]^+$, potentially explaining the lower SEE yield observed in [BMIM][BF_4] compared with [BMIM][Ac] despite sharing the same cation. This conclusion aligns with our calculations of the HOMO energies, showing that [BMIM][BF_4] has a lower HOMO value (and therefore a larger IP) compared to both [BMIM][Ac] and [EMIM][Ac].

4. Conclusions

In this work, we present SEE measurements of three imidazolium-based ionic liquids for primary electron beam energies ranging from 30 to 1000 eV. The low vapor pressure of ionic liquids allows for direct measurements of the SEE yield under vacuum by bombarding a liquid sample with electrons and measuring the resulting currents. The SEE yields of these ionic liquids vary considerably over the energy range studied, reaching maximum yields of around 2 at electron energies of 200 eV for [BMIM][Ac] and [EMIM][Ac], and

250 eV for [BMIM][BF_4]. Among the three, [BMIM][Ac] has the highest yield, while [BMIM][BF_4] has the lowest.

To explain these differences, molecular orbital calculations were performed. For [BMIM][Ac] and [EMIM][Ac], the electrons are likely donated from the acetate anion, whereas for [BMIM][BF_4], the electrons likely originate from the [BMIM]$^+$ cation. Since the electron donor site for both [BMIM][Ac] and [EMIM][Ac] is likely the same, and their HOMO energies are similar, the orientation of the alkyl chain may play an important role. The alkyl chain, which extends outward into the vacuum, could create a larger potential drop for longer chains, possibly explaining the higher yield of [BMIM][Ac] over [EMIM][Ac]. The low yield of [BMIM][BF_4] could be attributed to the high ionization potential of the likely electron donor, the [BMIM]$^+$ cation.

These findings are applicable for discharges using ionic liquid electrodes for plasma synthesis of nanoparticles and may enhance our understanding of how SEE occurs in liquids. The results of this study can be used for precise modeling of plasma discharges operating with imidazolium-based ionic liquid electrodes and for explaining the increased discharge currents observed with these electrodes.

Data availability statement

The data that support the findings of this study are either contained within this paper or available from the author upon reasonable request.

Acknowledgments

The author would like to thank Yevgeny Raitses, Alex Merzhevskiy, Tim Bennett, Angelica Ottaviano, Ian Reed, Pierce Wickenden, and Nick Lipari for productive discussions and their assistance with these measurements. This work was supported by the U.S. Department of Energy Award No. DE-SC0024655. Work at Princeton Collaborative Low Temperature Plasma Research Facility (PCRF) was supported by the U.S. Department of Energy under Contract No. DE-AC02-09CH11466. The authors also acknowledge use of the ELSA high performance computing cluster at The College of New Jersey for performing the computational work reported in this paper. This cluster is funded in part by the National Science Foundation under grant numbers OAC-1826915 and OAC-2320244. The authors would also like to thank Dr Joseph Baker for fruitful discussions and Shawn Sivy for maintaining the ELSA high performance computing cluster.

ORCID iDs

A M Capece https://orcid.org/0000-0003-4147-7174
A N Enriquez https://orcid.org/0009-0001-3993-0235

References

[1] Galinski M, Lewandowski A and Stepniak I 2006 *Electrochim. Acta* **51** 5567
[2] Greaves T L and Drummond C J 2008 *Chem. Rev.* **108** 206–37
[3] Kaneko T, Baba K and Hatakeyama R 2009 *Plasma Phys. Control. Fusion* **51** 124011
[4] Brettholle M, Höfft O, Klarhöfer L, Mathes S, Maus-Friedrichs W, El Abedin S Z, Krischok S, Janek J and Endres F 2010 *Phys. Chem. Chem. Phys.* **12** 1750–5
[5] Höfft O and Endres F 2011 *Phys. Chem. Chem. Phys.* **13** 13472–8
[6] Chen Q, Li J and Li Y 2015 *J. Phys. D: Appl. Phys.* **48** 424005
[7] Wei Z and Liu C-J 2011 *Mater. Lett.* **65** 353–5
[8] Janiak C 2015 *Top Organomet. Chem.* **51** 17–54
[9] Surviliene S, Eugenio S and Vilar R 2011 Chromium electrodeposition from [BMIMB]BF4 ionic liquid *J. Appl. Electrochem.* **41** 107–14
[10] Kim T Y, Yeon J H, Kim S R, Kim C Y, Shim J P and Suh K S 2011 Shape-controlled synthesis of silver crystals mediated by imidazolium-based ionic liquids *Phys. Chem. Chem. Phys.* **13** 16138–41
[11] Baba K, Kaneko T and Hatakeyama R 2009 *Appl. Phys. Express* **2** 035006
[12] Chen Q, Kaneko T and Hatakeyama R 2010 *J. Appl. Phys.* **108** 103301
[13] Horváth B, Donkó Z, Schulze J and Derzsi A 2022 *Plasma Sources Sci. Technol.* **31** 045025
[14] Horváth B, Daksha M, Korolov I, Derzsi A and Schulze J 2017 *Plasma Sources Sci. Technol.* **26** 124001
[15] Baba K, Kaneko T and Hatakeyama R 2007 *Appl. Phys. Lett.* **90** 201501
[16] Kaneko T, Baba K and Hatakeyama R 2009 *J. Appl. Phys.* **105** 103306
[17] Kaneko R T, Harada T, Chen Q and Hatakeyama R 2010 *TENCON 2010 IEEE Region 10 Conf.* (*Fukuoka, Japan*) pp 149–53
[18] Delgado H E, Elg D T, Bartels D M, Rumbach P and Go D B 2020 *Langmuir* **36** 1156–64
[19] Oyarzabal E and Tabares F L 2021 *Nucl. Mater. Energy* **27** 100966
[20] Kvon V, Oyarzabal R E, Zoethout E, Martin-Rojo A B, Morgan T W and Tabares F L 2017 *Nucl. Mater. Energy* **13** 21–27
[21] Wang H, Liu S, Huang K, Yin X, Liu Y and Peng S 2012 *Int. J. Electrochem. Sci.* **7** 1688–98
[22] Nazet A, Sokolov S, Sonnleitner T, Makino T, Kanakubo M and Buchner R 2015 *J. Chem. Eng. Data* **60** 2400–11
[23] IOLITEC n.d. 1-butyl-3-methylimidazolium acetate, >98% (available at: https://iolitec.de/en/node/290)
[24] Scholtz J J, Dijkkamp D and Schmitz R W A 1996 *Philips J. Res.* **50** 375
[25] Rivera-Rubero S and Baldelli S 2006 *J. Phys. Chem. B* **110** 4756–65
[26] Frisch M J *et al* 2016 *Gaussian 16, Revision A.03, (Gaussian Inc)*
[27] Polik W F and Schmidt J R 2021 Wiley interdiscip *Rev. Comput. Mol. Sci.* **12** e1554
[28] Gupta S K, Gupta A K and Yadav R K 2021 *Acta Phys. Pol.* A **140** 400–6
[29] Ilawe N V, Fu J, Ramanathan S, Wong B M and Wu J 2016 *J. Phys. Chem.* C **120** 27757–67
[30] Bardak F, Bardak C, Karaca C, Kose E, Bilgili S and Atac A 2022 *J. Mol. Liq.* **345** 117030
[31] Herbert J M 2015 *Rev. Comput. Chem.* **28** 391–517